Spin Waves throughout the Brillouin Zone of a Double-Exchange Ferromagnet

T. G. Perring,[1] G. Aeppli,[2,3] S. M. Hayden,[4] S. A. Carter,[3] J. P. Remeika,[3,*] and S-W Cheong[3]
[1]*ISIS Facility, Rutherford Appleton Laboratory, Oxon OX11 0QX, United Kingdom*
[2]*NEC, 4 Independence Way, Princeton, New Jersey 08540*
[3]*AT&T Bell Laboratories, Murray Hill, New Jersey 07974*
[4]*H. H. Wills Physics Laboratory, University of Bristol, Bristol BS8 1TL, United Kingdom*
(Received 4 October 1995)

We use inelastic neutron scattering to measure the spin wave dispersion throughout the Brillouin zone of the double-exchange ferromagnet $La_{0.7}Pb_{0.3}MnO_3$. Magnons with energies as high as 95 meV are directly observed and an unexpectedly simple Heisenberg Hamiltonian, with solely a nearest-neighbor coupling of 8.79 ± 0.21 meV, accounts for the entire dispersion relation. The calculated Curie temperature for this local moment Hamiltonian overestimates the measured Curie point (355 K) by only 15%. Raising temperature yields unusual broadening of the high frequency spin waves, even within the ferromagnetic phase. [S0031-9007(96)00516-9]

PACS numbers: 71.27.+a, 75.30.Ds, 75.50.Cc

The past few years have witnessed a great revival [1] in the study of doped rare-earth perovskite manganites [2], $R_{1-x}X_SMnO_3$ (R = La, Pr, Nd and X = Ca, Ba, Sr, Pb), because of the colossal magnetoresistance effects that have been observed. A thousandfold decrease in resistivity in an applied field has been reported for thin films of $La_{0.67}Ca_{0.33}MnO_3$, for example, and there is strong interest in these materials because of both potential technological applications and fundamental questions relating to metallic band formation. The parent compounds are insulating antiferromagnets [3], such as $La^{3+}Mn^{3+}O_3{}^{2-}$, into which carriers can be introduced by chemical substitution onto the lanthanide sites with X^{2+}. With sufficient doping, the compounds can become metallic ferromagnets which undergo transitions to paramagnetic states at Curie points T_C comparable to room temperature. A large decrease in electrical conductivity, σ, which appears to be controlled solely by the field and temperature-dependent magnetization M, accompanies these transitions [4,5]. Of greatest recent interest is that near T_C the magnetic susceptibility is high so that σ as well as M is very field sensitive.

The experimental [2,3] and theoretical [4–6] study of the bulk properties of the doped manganites has a long and distinguished history. The properties of $La_{1-x}{}^{3+}X_x{}^{2+}(Mn_{1-x}{}^{3+}Mn_x{}^{4+})O_3{}^{2-}$ are usually explained by double-exchange theory [4]. Crystal fields split the Mn $3d$ orbitals into three localized T_{2g} orbitals, and two higher energy E_g orbitals which are strongly hybridized with the oxygen p orbitals. Each Mn ion has a core spin of $S = 3/2$, and a fraction $(1 - x)$ have an extra electron in the E_g orbitals with spin parallel to the core spin due to strong intrasite exchange. The electron can hop to an adjacent Mn site with unoccupied E_g orbitals without loss of spin polarization [4], but with an energy penalty that varies as the cosine of half the angle between the core spins. The model accounts qualitatively for ferromagnetic ordering and carrier mobility that depends on the relative orientation of the Mn moments, which near T_C will therefore be strongly dependent on the applied magnetic field.

Surprisingly, to the best of our knowledge, there exist no measurements [7,8] of the magnetic dynamics throughout the Brillouin zone in any of the ordered magnetic states of these materials. The spectrum of magnetic excitations is unique as a source of answers to questions as fundamental as whether a simple local moment model is appropriate for the magnetic dynamics and what the effective Hamiltonian and corresponding coupling constants are. We have therefore used inelastic neutron scattering to measure the magnetic excitations between 10 and 100 meV in $La_{0.7}Pb_{0.3}MnO_3$, a metallic ferromagnet with $T_C = 355$ K. At 10 K, there are clearly resolved spin waves up to the zone boundary along all major symmetry direction. A ferromagnetic Heisenberg Hamiltonian, including only a nearest-neighbor coupling which yields an overall magnon bandwidth of 108 meV, is sufficient to describe the data as well as, to within 15%, the Curie temperature of the compound. This simplicity of the effective spin Hamiltonian for $La_{0.7}Pb_{0.3}MnO_3$ is surprising given that the parent compound $LaMnO_3$ is an antiferromagnet and that there are strong interactions between carriers and magnetic moments as evidenced by the collapse of the electrical resistivity below T_C. On warming, however, the carriers clearly manifest themselves in the second discovery of our research, the heavy damping of very high-frequency ($\approx$100 meV) spin waves even below T_C.

The sample used in our measurements is a 1.86 g single crystal of $La_{0.7}Pb_{0.3}MnO_3$ grown from a lead oxide flux [9]. Crystals such as this have a slight rhombohedral distortion at low temperatures. However, given the twinning of our crystal and the resolution of the neutron experiment, we take the sample to be cubic with lattice constant $a_0 = 3.9$ Å [9], equal to the Mn-Mn ion separation. We have measured the temperature-dependent resistivity ρ and low-field magnetization M for a small

sample from the same growth batch. M rises sharply below $T_C = 355$ K, and there is a concomitant drop in ρ, as is typical for $LaMnO_3$ samples doped to achieve ferromagnetism. Using magnetic neutron diffraction [3] we have confirmed that T_C is also 355 K for the larger crystal used for our inelastic experiments.

We performed the neutron scattering measurements using the HET spectrometer at the pulsed spallation source ISIS of the Rutherford Appleton Laboratory. HET is a direct geometry time-of-flight spectrometer [10], with a Fermi chopper in front of the sample whose phase with respect to the pulse can be chosen to fix the incident beam energy at any desired value. The neutron flight times give the energies of the scattered neutrons, and hence the energy transfers $\hbar\omega$. Together with the scattering angle and the sample orientation, they also yield the momentum transfers $\mathbf{Q}$. One method for examining the dispersion surfaces of the normal modes of single crystals with triple-axis spectrometers is to plot the experimental intensities as a function of momentum transfer along some symmetry direction for fixed energy transfer. Given a multidetector chopper spectrometer with fixed incident energy E_i, it is possible to measure scans along symmetry direction without rotating the sample [10]. In general, the energy transfer will vary along these directions. Even so, with a judicious choice of E_i and sample orientation, one can achieve scans along the chosen directions for which the energy transfer is almost constant, as illustrated in Fig. 1(a). Near reciprocal lattice points this yields a pair of peaks corresponding to counterpropagating modes with wave numbers specified by the intersection of the surfaces defined by the nearly constant $\hbar\omega$ scan and the dispersion relation.

Figure 1(b) shows data for a scan centered on $\hbar\omega = 18$ meV obtained along the $(1, 1, 0)$ direction for our sample of $La_{0.7}Pb_{0.3}MnO_3$ at 10 K. As for the analogous triple-axis scan, the slightly different shapes and intensities of the two peaks are due to resolution effects which are well understood, as indicated by the excellent agreement between the data and the solid line representing the convolution of the instrumental response function and the theoretical cross section for spin waves in a nearest-neighbor exchange coupled Heisenberg ferromagnet. To allow for possible damping processes, for example, decay into electron-hole pairs, the spin wave cross section has been convolved with a damped simple harmonic oscillator. This reduces to delta functions in the limit of light damping.

We have used several incident beam energies (50, 100, and 200 meV) and sample orientations to obtain data such as those in Fig. 1(b) along all major symmetry directions. The locus of peaks from a sufficiently large number of scans provides complete knowledge of the dispersion relation. Figure 2 shows the outcome of our survey, which reveals a net magnon bandwidth of approximately 100 meV. Figure 3(a), which presents classic time-of-flight scans for two fixed detector angles, demonstrates

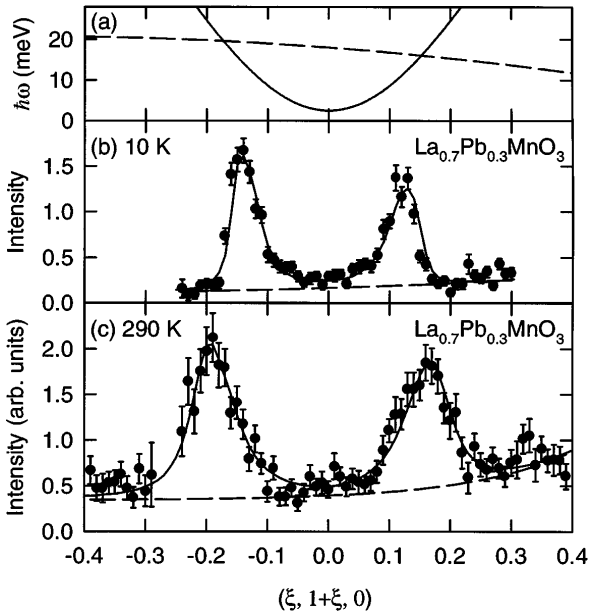

FIG. 1. (Nearly) constant-$\hbar\omega$ scan for $E_i = 50$ meV and crystal orientated with $(-1, 1, 0)$ parallel to the incident beam. (a) $\hbar\omega$ as a function of momentum transfer (dotted line) and magnon dispersion surface (continuous line) for the scan. Scattered intensity peaks are expected where the two intersect. Frames (b) and (c) show the scattering cross section for $T = 10$ and 290 K, respectively, normalized to have the same intensity scale. The different intensities of corresponding peaks in the two frames arise from the Bose occupation factor. Data collection times: 8 h at 170 μA proton current with (b) U target and (c) Ta target.

that the high energy magnons (solid circles) near the $(\frac{1}{2}, \frac{1}{2}, \frac{1}{2})$ zone boundary point are well defined at 10 K. This implies that well within the ferromagnetic and metallic phase, there is little damping of the spin waves via interactions with the carriers. As a technical aside, note that as in Fig. 1 the two peaks in Fig. 3 (solid circles) rise from the intersection of the neutron phase-space trajectory with the spin wave dispersion surface near a high symmetry point. We are thus, again as in Fig. 1, seeing counterpropagating magnons on either side of such

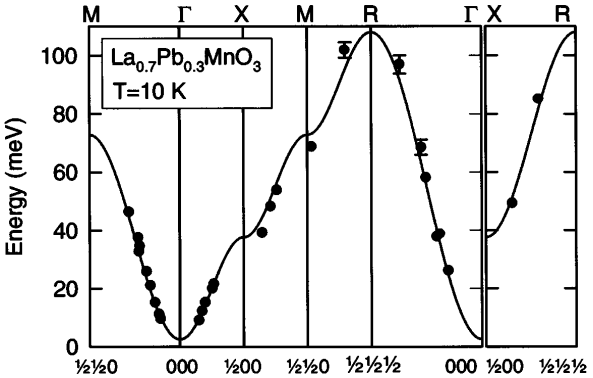

FIG. 2. Measured spin wave dispersion along all major symmetry directions at 10 K. The error bars are smaller than the points except where shown. Solid lines show the dispersion relation for a Heisenberg ferromagnet with nearest-neighbor coupling that best fits the data (see text).

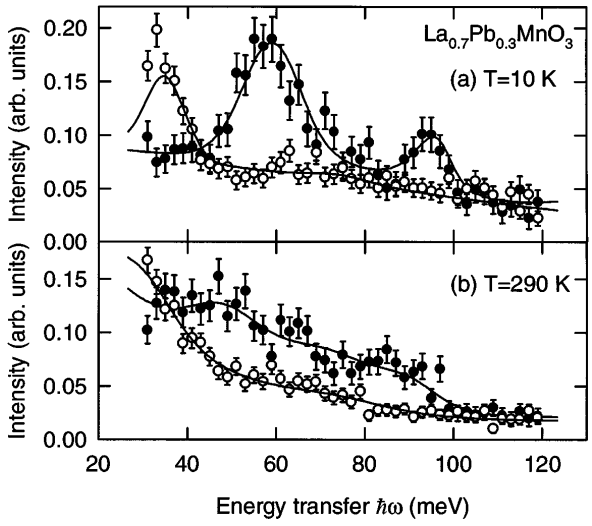

FIG. 3. Energy scans obtained for fixed $E_i = 200$ meV by integrating over the scattering angle ranges $2\theta = 9.31° - 10.56°$ (closed circles) and $2\theta = 15.56° - 17.43°$ (open circles). The data are normalized by detector solid angle. Frames (a) and (b) show the scattering cross section obtained for $T = 10$ and 290 K, respectively, normalized to have the same intensity scale. The solid lines in each frame are the results of the fit to a damped simple harmonic oscillator as described in the text.

a point, in this case the $(\frac{1}{2}, \frac{1}{2}, \frac{1}{2})$ zone boundary point rather than the $(0, 1, 0)$ zone center. For the higher angle scattering (open circles), the momentum transfers are far away from $(\frac{1}{2}, \frac{1}{2}, \frac{1}{2})$, so that the data are representative of the nonmagnetic scattering for $\hbar\omega > 45$ meV. Below 45 meV, there is spin wave scattering which, using the model described below, can be understood simultaneously with the high energy modes.

One of the major open questions in the field of the doped manganites concerns the appropriate effective spin Hamiltonian in the ordered state. A general candidate is the Heisenberg form with couplings J_{ij} between pairs of spins at sites $\mathbf{R}_i$ and $\mathbf{R}_j$,

$$H = -\sum_{ij} J_{ij} \mathbf{S}_i \cdot \mathbf{S}_j \,. \tag{1}$$

For a ferromagnetic ground state, the corresponding spin wave dispersion relation is

$$\hbar\omega(\mathbf{Q}) = \Delta + 2S(J(\mathbf{0}) - J(\mathbf{Q})) \,, \tag{2}$$

where

$$J(\mathbf{Q}) = \sum_j J_{ij} e^{i\mathbf{Q}\cdot(\mathbf{R}_i - \mathbf{R}_j)} \,. \tag{3}$$

In Eqs. (2) and (3) we have specialized to the case of a Bravais lattice, so that $J(\mathbf{Q})$ is independent of which site $\mathbf{R}_i$ is chosen as the origin. Also, we have followed common practice and included a constant offset Δ to account for small anisotropies. Equation (2) reduces to the well-known form $\hbar\omega(\mathbf{Q}) = \Delta + Dq^2$ in the $q \to 0$, long wavelength, limit, where the stiffness D is a weighted average over all the exchange constants, $D = (S/3)\sum_j J_{ij}|\mathbf{R}_i - \mathbf{R}_j|^2$ for a cubic material. Given that the parent compound $LaMnO_3$ is antiferromagnetic, we anticipated needing to include at least several terms in the Fourier series, Eq. (3), to account for the ensuing complexity of the effective interactions in $La_{0.7}Pb_{0.3}MnO_3$. More specifically, we expected softness in the spin wave spectrum near zone boundary points such as $(\frac{1}{2}, 0, 0)$, $(\frac{1}{2}, \frac{1}{2}, 0)$, and $(\frac{1}{2}, \frac{1}{2}, \frac{1}{2})$. Such softness is not observed. Indeed, a single ferromagnetic nearest-neighbor coupling $2J_1S = 8.79 \pm 0.21$ meV, yielding the dispersion relation

$$\hbar\omega(\mathbf{Q}) = \Delta + 4J_1S(3 - \cos(q_x a_0) - \cos(q_y a_0) - \cos(q_z a_0)) \tag{4}$$

is entirely sufficient to account for the data in Fig. 2. Our fits also yield a small value for the effective gap $\Delta = 2.51 \pm 0.46$ meV, which is well below the low frequency cutoff of our measurements which have been restricted to incident neutron energies of 50 meV and above. Adding second and third nearest-neighbor exchange constants J_2 and J_3 does not improve the fit. The values obtained are $2J_2S = -0.09 \pm 0.24$ meV (second nearest neighbor only), and $2J_2S = -0.43 \pm 0.35$ meV, $2J_3S = 0.44 \pm 0.36$ meV (second and third nearest neighbor), with small changes in each case to the values of J_1 and Δ similar to the errors in these quantities.

We have established that the effective Hamiltonian for the spins in $La_{1-x}Pb_xMnO_3$ with $x = 0.3$ is that for a simple cubic Heisenberg ferromagnet with a single nearest-neighbor coupling. The mean field value for the Curie temperature is $4J_1S(S + 1)/k_B$ or, in terms of the magnon bandwidth, $E_{ZB}(S + 1)/6k_B$, where $E_{ZB} \equiv 24J_1S \equiv \hbar\omega(\mathbf{Q} = (1/2, 1/2, 1/2))$. For S we use the mean spin on the manganese ions, $S = 3/2 + (1 - x)/2 = 1.85$, as suggested by the double-exchange theory [4–6], and which correctly gives the measured magnetization at $T = 0$ K [11]. Together with our measured value of $2J_1S$, we calculated a mean field $T_C^{\mathrm{MF}} = 581$ K for our sample. It is well known that fluctuations reduce the Curie temperature from T_C^{MF} even for three-dimensional local moment ferromagnets. In particular, for the simple cubic nearest-neighbor Heisenberg ferromagnet, fluctuations reduce T_C to $(J_1/k_B)[2.90S(S + 1) - 0.36]$ [12]. When we evaluate this quantity, again with $S = 1.85$ and the measured value of $2J_1S$, the expected Curie temperature is 410 K, only 15% larger than the measured value of 355 K.

Both because of the consistency of the Curie temperature with the magnon bandwidth and because of the simplicity of the low temperature spin waves, $La_{0.7}Pb_{0.3}MnO_3$ appears to be a very conventional ferromagnet. More specifically, since an effective spin Hamiltonian containing only nearest-neighbor couplings describes our neutron data, theoretical procedures which average the carrier motion over many bonds seem to be correct for $La_{1.7}Pb_{0.3}MnO_3$. The validity of such averaging would also mean that the transport properties simply follow the magnetization, as is

actually suggested by zero-frequency (i.e., static) bulk experiments [5,6]. Inelastic neutron scattering affords an opportunity to test whether in the dynamics of the magnetism the conduction electrons play a less trivial role, especially as T_C is approached. It turns out the raising temperature within the ferromagnetic phase has a dramatic effect on the high frequency magnons. Figure 3(b) shows that these excitations broaden to the point of virtually disappearing on warming from 10 to 290 K, over which range the ferromagnetic order has changed relatively little [$M(T)/M(0) = 0.75$ at $T/T_C = 0.8$ [5]]. Both the 10 and 290 K spin waves were fitted to the convolution of the instrumental resolution and a damped simple harmonic oscillator, with eigenfrequencies determined by Eq. (2), with J allowed to vary but with Δ constrained to zero. The fitted inverse lifetime γ for the high frequency magnons increases from 10 ± 2 meV at 10 K to 27 ± 5 meV $\approx k_B T$ at 290 K. In contrast, the lower energy magnons shown in Fig. 1(b) remain well defined, with γ increasing only to 5 ± 1 meV. In the classic insulating ferromagnet EuO, the magnons remain much better defined throughout the Brillouin zone even at similar reduced T/T_C [13]. For example, at the $(\frac{1}{2}, \frac{1}{2}, \frac{1}{2})$ point of this (face centered) cubic material and $T/T_C = 0.86, \gamma = 0.1 k_B T$. It therefore appears that the same scattering mechanisms responsible for the many unusual bulk attributes of the manganites are at work to heavily damp the high frequency magnons even below T_C in $La_{0.7}Pb_{0.3}MnO_3$. That higher frequency properties are still evolving below T_C even when low frequency quantities are already tending towards saturation is also clear in the frequency-dependent optical conductivity recently reported for $La_{1-x}Sr_xMnO_3$ [14].

We have carried out the first measurement of the spin waves outside the small-q regime for a metallic perovskite manganite. The outcome is that at low temperatures there are well-defined spin waves throughout the Brillouin zone. The dispersion relation is that for a simple cubic ferromagnet with one significant free parameter, an effective nearest-neighbor Heisenberg coupling, which also accounts for the Curie temperature of the material to within 15%. This represents an unexpected and extraordinary simplification of the spin physics in a material whose parent compound is an antiferromagnetic insulator. One could well have expected that the interactions responsible for the latter might become apparent at short wavelengths in the ferromagnet. Indeed, in the superconducting cuprates, the magnetic fluctuations possess a much more complex wave-vector dependence [15] with certain short-wavelength features [16] inherited from the parent antiferromagnets. Furthermore, many insulating ferromagnets such as EuS and EuO, and classic itinerant ferromagnets [17] ranging from Ni to Pd_3Fe, have more complicated low temperature spin waves. That analogous complexity is not found at 10 K in our manganite means that the only role of the charge carriers, as far as the low T and low ω properties are concerned, is to fix a single effective exchange constant. However, our measurements are the first to show that in high T and high ω they acquire a more interesting role, that of heavily damping the spin waves near the zone boundary.

We are grateful to P. B. Littlewood, A. Millis, H. A. Mook, A. P. Ramirez, Y. Tokura, and C. M. Varma for helpful discussions.

*Deceased.

[1] See, e.g., R. M. Kusters *et al.,* Physica (Amsterdam) **155B**, 362 (1989); R. von Helmolt *et al.,* Phys. Rev. Lett. **71**, 2331 (1993); K. Chahara *et al.,* Appl. Phys. Lett. **63**, 1990 (1993); S. Jin *et al.,* Science **264**, 413 (1994); A. Asamitsu *et al.,* Nature (London) **373**, 407 (1995).

[2] G. H. Jonker and J. H. van Santen, Physica (Vtrecht) **16**, 337 (1950); J. H. van Santen and G. H. Jonker, Physica (Vtrecht) **16**, 599 (1950).

[3] E. O. Wollan and W. C. Koehler, Phys. Rev. **100**, 545 (1955).

[4] C. Zener, Phys. Rev. **82**, 403 (1951); P. W. Anderson and H. Hasegawa, Phys. Rev. **100**, 675 (1955); P.-G. de Gennes, Phys. Rev. **118**, 141 (1960).

[5] C. W. Searle and S. T. Wang, Can. J. Phys. **48**, 2023 (1970); .

[6] Recent theory is by N. Furukawa, J. Phys. Soc. Jpn. **63**, 3214 (1994); comparison with experiment is given by Y. Tokura *et al.,* J. Phys. Soc. Jpn. **63**, 3931 (1994).

[7] The spin wave stiffness found in the present work has been reported by A. Millis *et al.,* Phys. Rev. Lett. **74**, 5144 (1995).

[8] After we carried out the research described in this paper, A. Millis made us aware of a preprint by M. C. Martin *et al.,* who describe neutron measurements of spin waves in the long-wavelength limit for $La_{1.7}Sr_{0.3}MnO_3$.

[9] A. H. Morrish *et al.,* Can. J. Phys. **47**, 2691 (1969).

[10] C. G. Windsor, *Pulsed Neutron Scattering* (Taylor and Francis, London, 1981). Chopper spectrometers are in quite common use for investigations of dispersive magnetic excitations in single crystals. See, e.g., T. G. Perring *et al.,* J. Appl. Phys. **69**, 6219 (1991); S. M. Hayden *et al.,* Phys. Rev. Lett. **67**, 3622 (1991); D. A. Tennant *et al.,* Phys. Rev. Lett. **70**, 4003 (1993); S. Itoh *et al.,* Phys. Rev. Lett. **74**, 2375 (1995); T. G. Perring *et al.,* Physica (Amsterdam) **213B & 214B**, 348 (1995).

[11] L. K. Leung *et al.,* Can. J. Phys. **47**, 2697 (1969).

[12] G. S. Rushbrooke *et al.,* in *Phase Transitions and Critical Phenomena,* edited by C. Domb and M. S. Green (Academic, New York, 1974), Eq. (5.4).

[13] H. A. Mook, Phys. Rev. Lett. **46**, 508 (1981).

[14] Y. Okimoto *et al.,* Phys. Rev. Lett. **75**, 109 (1995).

[15] T. R. Thurston *et al.,* Phys. Rev. B **40**, 4585 (1989); S-W. Cheong *et al.,* Phys. Rev. Lett. **67**, 1791 (1991).

[16] T. Imai *et al.,* Phys. Rev. Lett. **70**, 1002 (1993); S. M. Hayden *et al.,* Phys. Rev. Lett. **76**, 1344 (1996); K. Yamada *et al.* (to be published).

[17] For reviews, see articles by H. A. Mook and P. A. Lindgård, in *Spin Waves and Magnetic Excitations,* edited by A. S. Borovik-Romanov and S. K. Sinha (North-Holland, Amsterdam, 1988), Vol. 22.